Hindawi
International Journal of Aerospace Engineering
Volume 2018, Article ID 7286705, 12 pages
https://doi.org/10.1155/2018/7286705

Research Article

Effect of Airflow Temperature on the Formation of Initial Flame Kernel and the Propagation Characteristics of Flame

Jianzhong Li,[1] **Jian Chen**,[1] **Li Yuan**,[2] **and Ge Hu**[1]

[1]*Key Laboratory of Aero-engine Thermal Environment and Structure, Ministry of Industry and Information Technology, Nanjing University of Aeronautics and Astronautics, 29 Yudao St., Nanjing 210016, China*
[2]*School of National Defense Engineering, The Army Engineering University of PLA, 88 Biaoying Rd, Nanjing, 210007 Jiangsu, China*

Correspondence should be addressed to Jianzhong Li; ljzh0629@nuaa.edu.cn

Received 14 February 2018; Revised 9 September 2018; Accepted 19 September 2018; Published 17 December 2018

Academic Editor: Linda L. Vahala

Using liquid RP-3 aviation kerosene as the fuel to study, the effect of airflow temperature on the formation of initial flame kernel during the ignition of spray combustion and on the propagation characteristics of flame was investigated. Combining high-speed camera and dynamic temperature acquisitions at the outlet of combustor, the internal triggering mode was used under a constant fuel flow rate and airflow velocity. This combined system simultaneously recorded the formation of initial flame kernel, flame propagation, and outlet temperature variation of combustor under different airflow temperatures. MATLAB software was used to obtain the reaction zones at different moments and to analyze the effects of airflow temperature on morphological characteristics such as flame area, perimeter-to-area ratio, maximum length-to-height ratio, equivalent mean length-to-height ratio, mass center, and centroid. According to the growth rate in flame area, the ignition process can be divided into three stages: formation of flame kernel, rapid development of flame, and stable development of flame. Airflow temperature not only affects the formation time of flame kernel but also affects the growth rate of flame area. During the development of flame, the movements of mass center and centroid are irregular, and their positions do not coincide with each other. However, the overall moving trends are consistent. With the increase of the airflow temperature, the position, where the flame kernel is gradually formed, moves closer to the center of the end face of spark plug. The force of airflow on flame is the main factor that increases the flame area and heat-release rate. Therefore, the folds around the flame edge mainly result from the stretching under the action of airflow. With the increase in airflow temperature, the heat release of the initial flame kernel increases, and the ratio of perimeter to area as a characterization parameter increases by 8%, 86%, and 33%, respectively. In addition, the maximum outlet temperature rise increased by about 53%, 73.5%, and 0.65%, respectively. Meanwhile, the maximum rate of temperature rise increased by about 42.8%, 57%, and 5.1%, respectively.

1. Introduction

The ignition for spray combustion of a liquid fuel is a key process in propulsion systems and thermal energy conversion equipment. Especially for aeroengines, the ignition will directly affect the safety and reliability. Therefore, the ground and high-altitude ignition performance of aeroengines is listed as one of the important performance indicators. The ignition process in the spray combustion of a liquid fuel is much more complex than that of a gaseous mixture. For the ignition in the spray combustion of a liquid fuel, the volatility of fuel, droplet size, equivalence ratio, and preevaporated extent are important factors which are different from the ignition in the combustion of a gaseous fuel [1]. Therefore, the ignition in the spray combustion of a liquid fuel can be divided into three different ignition states: droplet ignition, droplet group ignition, and spray ignition [2]. Because of the complexity and importance of spray ignition of a liquid fuel, numerous studies have been conducted over the years, and the key factors that affect the ignition performance and improved ignition measures have been determined [3–11].

Although numerical simulations provide a suitable, reasonable, and microscopic explanation of the flame propagation mechanism and chemical reaction kinetics during the spray ignition [12–16], they cannot provide a valid and an accurate prediction of ignition because of the complex nature of simultaneous droplet evaporation and mixing and the coupling of airflow and chemical reactions. The continuous development in modern optical measurement technology have laid the foundation for further exploration of the flame propagation mechanisms and flame structures during the ignition of spray combustion. Naegeli and Dodge [17] experimentally studied the ignition characteristics of T63 engine. The ignition delay phenomenon was recorded using a high-speed camera, and the effects of viscosity, volatility, and atomization characteristics of fuel on the ignition performance were evaluated. Ahmed and Mastorakos [18] studied the ignition of methane jet flame using a high-speed camera and planar laser-induced fluorescence of OH radicals. After the initial spherical flame kernel was formed, the flame propagated upstream in the form of a cylindrical surface. Marchione et al. [19, 20] experimentally studied the ignition and ignition characteristics of spray combustion of *n*-heptane. High-speed camera images showed that the propagation characteristics of flame in the upstream determined the success or failure of ignition. Oldenhof et al. [21] used an intensified high-speed camera to investigate the formation and uplifting behavior of initial flame kernel of high-temperature flame with a continuous flow and found an essential difference when comparing with the traditional flame lifting caused by the cocurrent flow and jet of cold air. Using high-speed camera and thermocouple measurement system, Chen et al. Investigated the influence of airflow pressure on the process and performance of ignition [22]. But, in that study, the effect of airflow temperature on ignition characteristics was not involved.

Although several factors affect the spray ignition performance of a liquid fuel, it is expected that an optimum droplet size and fuel/air ratio that can minimize the ignition energy and can lead to the shortest ignition delay time exist. In addition, the optimum droplet size, fuel/air ratio, and volatility of fuel are mutually restrained [23]. Variations in airflow temperature change the air density and evaporation rate of fuel, thus affecting the droplet distribution and fuel/air ratio in ignition and leading to differences in ignition performance. At the same time, the airflow temperature also affects the ignition delay time [24], combustion velocity [25], and heat and mass transfer during the flame propagation [26]. Therefore, variations in airflow temperature will directly or indirectly affect the spray ignition performance. However, the effect of airflow temperature on the morphological characteristics of flame during spray ignition has been rarely reported. In addition, the air temperature could also have an important effect on other areas of combustion, such as combustion efficiency [27], emissions [28], and specific impulse of propulsion system [29]. Therefore, it is very necessary to study the influence of airflow temperature on combustion process and performance, which has a certain guiding significance for improving the optimization design of burner and propulsion system.

In order to improve the ignition performance of a slinger combustor with indirect ignition and to supplement the experimental data of the influence of air temperature on them, under atmospheric pressure, the formation of initial flame kernel and the propagation characteristics of flame during the ignition of the liquid fuel spray combustion were investigated by combining high-speed camera and dynamic temperature acquisitions at the exit of combustor. The airflow parameters ($V_0 = 10$ m/s, $T_0 = 308$ K, 343 K, 373 K, and 393 K) were determined by ignition conditions, and the RP-3 liquid aviation kerosene was used as the fuel for a turboshaft engine. The power of the turboshaft engine is 500~600 KW. MATLAB software was used to obtain the reaction zones at each moment and to analyze the effect of airflow temperature on morphological characteristics such as the flame area, perimeter-to-area ratio, maximum length-to-height ratio, equivalent mean length-to-height ratio, mass center, and centroid. The formation of initial flame kernel and the propagation of flame were evaluated to determine the effect of airflow temperature on the formation of initial flame kernel, propagation characteristics of flame, starting time of outlet temperature increase, maximum temperature increase time, and temperature increase rate.

2. Experiment Description

The ignition experimental system for spray combustion is shown in Figure 1. The system mainly includes an air supply system, a fuel supply system, an ignition system, a control system, an air heater, a rectangular combustor, a thermocouple, a high-speed camera, and a temperature acquisition system. The combustor is a rectangular structure, which simplified the structure of a slinger combustor, but it is necessary to ensure that the airflow passage is the same as the actual situation, as shown in Figure 2. The combustor has a total length of 455 mm and inlet and outlet areas of $120 \times 85\ \text{mm}^2$. One window with an area of 75×50 mm2 was set at one side of the combustor for optical measurements. The installation position of the pressure-swirl atomizer and ignition plug is also the same as the real state. A pressure-swirl atomizer and center of spark plug were mounted on the same cross-section with an intersection angle of 14°. The spray angle of the pressure-swirl atomizer is 52°. The spark energy of the ignition plug is 0.4 J. Three thermocouples were installed on the same section at the outlet of the combustor, 250 mm away from the axis of spark plug. The first thermocouple (TC-1) was 20 mm (1/4H) away from the upper wall of the combustor. The second thermocouple (TC-2) was 42.5 mm (1/2H) away from the upper wall of the combustor. The third thermocouple (TC-3) was 65 mm (3/4H) away from the upper wall of the combustor. In the experiment system, the airflow was supplied by a single-screw compressor. The air was first heated using an electric heater before entering the combustor. The airflow rate and temperature were measured using a vortex flowmeter and thermocouple in front of the inlet of the combustor, respectively. Before each set of experiments, the temperature of air heater was preset, and the airflow rate in the combustor

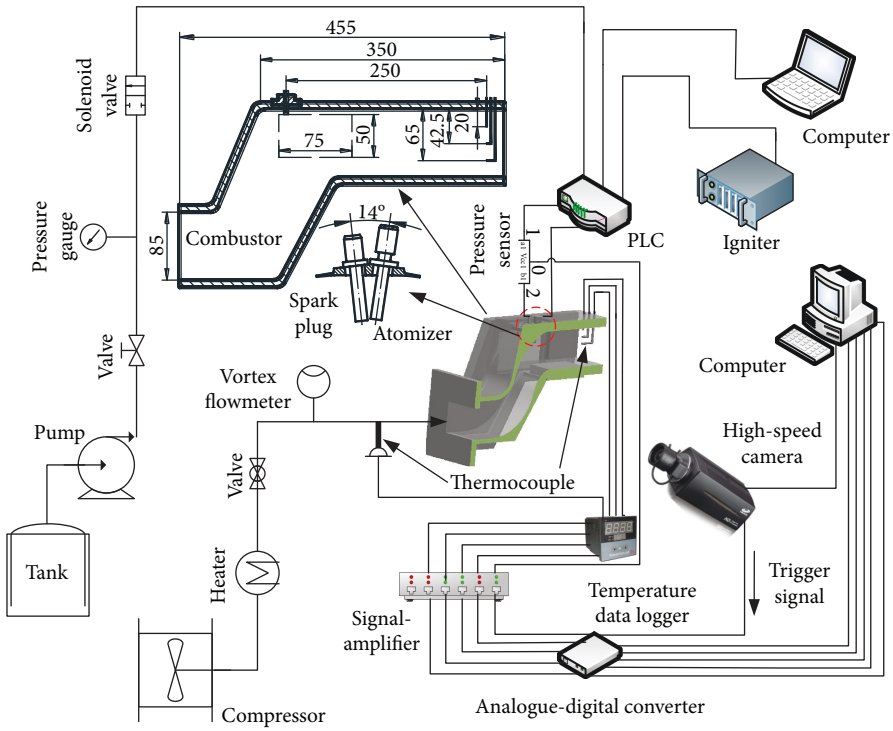

Figure 1: Schematic of ignition experimental system for spray combustion.

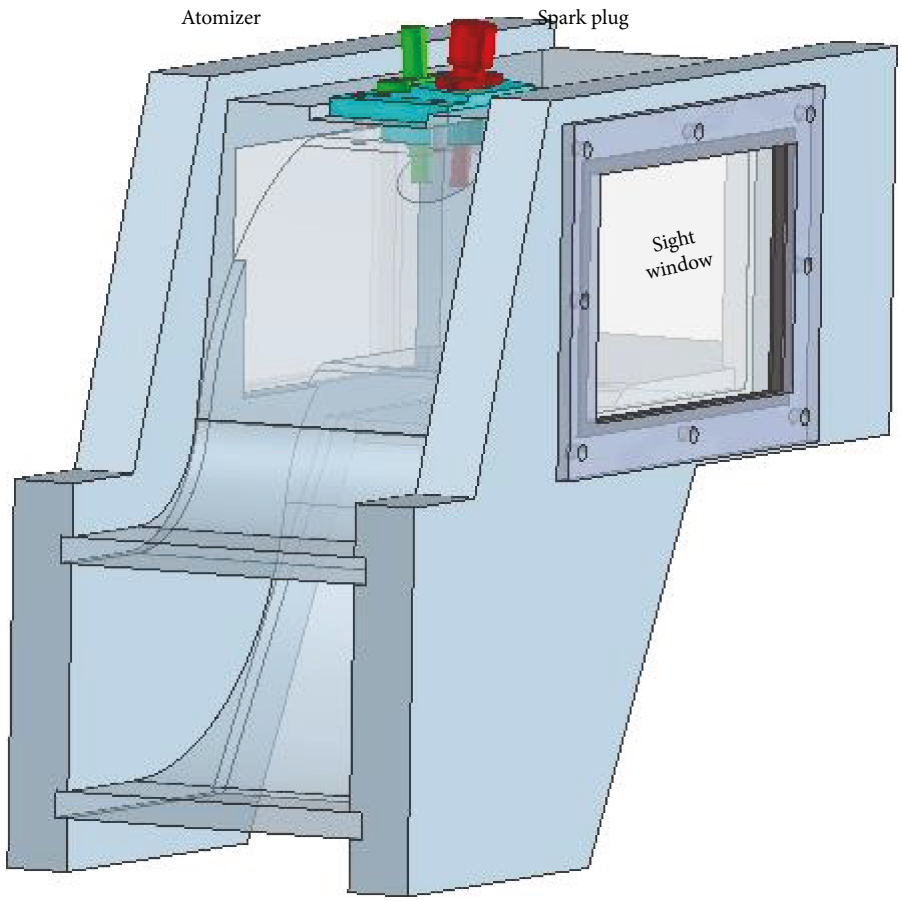

Figure 2: Rectangular structure combustor.

was regulated. When the inlet temperature of the combustor reached the requirements of experimental conditions, the ignition experiment was carried out. To avoid the effect of high-temperature burned gas and wall temperature of combustor on the next set of experiments, the combustor was cold-blown for 5 to 10 min between each two sets of tests. After the temperature was stable and satisfied the experimental requirements, the following tests were carried out. The fuel supply pressure was simultaneously measured using a pressure gauge in front of a solenoid valve and pressure sensor in front of the nozzle. To ensure synchronization between the high-speed camera and temperature acquisition system, the internal triggering mode of the outlet temperature acquisition system of combustor was used. It was triggered by the voltage signal produced by the starting of high-speed camera. The temperature acquisition time was 8 s. A high-speed camera (Y5 series high-speed camera, Integrated Device Technology, USA) was used. The camera has a maximum resolution of 2336×1728 pixels, maximum sensitivity of 3000 ISO, and maximum frame rate of 6900 fps. In the experiment, the resolution of high-speed camera was set at 1150×1112 pixels, and the shooting speed of camera at this setting was 1000 fps. Before the shooting, the focal length of the camera was adjusted to the center plane of spark plug, and the size was calibrated using the shooting scale. The calculated pixel magnification was 0.0449 mm/pixel.

To ensure the coordination of a fuel supply system and an ignition system, a programmable logic controller (PLC) was used to control the systems. The fuel supply and ignition systems were simultaneously turned on and switched off after 3 s. The moments of turning on and switching off were acquired in the voltage signals using a computer. The injection moment of atomizer was acquired from the output signal of pressure sensor in front of the atomizer. The discharge moment of spark plug was obtained using the high-speed camera, as shown in Figure 3, where t_{open} is the opening moment of fuel supply and ignition systems, t_{close} is the closing moments of fuel supply and ignition systems, Δt_w is the working time of fuel supply and ignition systems, t_f is the injection time of atomizer, t_{ig} is the discharging moment of spark plug, t_{end} is the ending moment of acquisition process, t_{start} is the moment when the thermocouple exhibits a temperature increase, t_{max} is the moment when the thermocouple exhibits the maximum temperature, Δt_{ig} is the time difference between the data acquisition and discharge of spark plug, and Δt_{start} and Δt_{max} are the time difference between the temperature increase and discharge moments of spark plug and between the injection and discharge moments of spark plug, respectively, where Δt_f is the fuel supply pressure difference ΔP_L and Δt_p is the ignition energy. According to the experimental results, when ΔP_L was 0.5 MPa and ignition energy was 0.4 J, $\Delta t_f = 0.546 \pm 0.001$ s and $\Delta t_p = 0.622 \pm 0.001$ s.

3. Results and Discussion

During the ignition test, the development of flame was photographed using a high-speed camera and stored as a grayscale image, as shown in Figure 4(a). To highlight the details and boundary of flame, the original image was filtered and pseudocolorized using MATLAB software, and the processed image is shown in Figure 4(b). During its development, the flame exhibits an irregular structure and nonuniform brightness distribution. Therefore, it is not necessary to reasonably extract the flame's contour and analyze its shape and trajectory. In this study, the image was segmented, and the flame's boundary contour was extracted using the method of maximum intercluster variance method (known as Otsu's method, a self-adaptive threshold determination method). The flame's structural parameters such as area, perimeter, length, and height of flame as well as the trajectories of mass center and centroid were calculated within the contour of flame [30], as shown in Figure 4(c). To reduce the calculation error, during the calculation of mass center and centroid of the flame, the origin of coordinates was selected as the starting point at the upper-right corner of the picture. The direction along the axial downstream direction of combustor was defined as the positive direction of X-axis, and the downward direction along the height of combustor was defined as the positive direction of Y-axis.

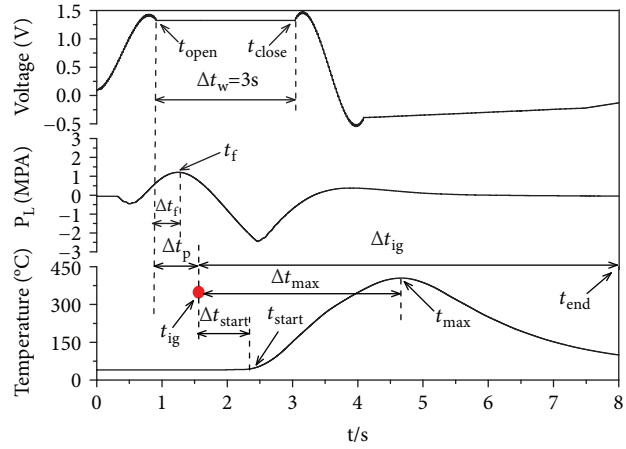

Figure 3: Definition of ignition times.

The initial flame kernel formation and flame propagation in the ignition of spray combustion at different inlet temperatures are shown in Figure 5, where $t = 0$ ms represents the image before the igniting. The spark plug sparked successfully when $t = 1$ ms. Then, the initial flame kernel rapidly formed during the chemical reaction with the nearby combustible gas. The maintenance for the self-living and development of initial flame kernel requires continuous intensified heat liberation. Then, the fire flame kernel is gradually stretched. At this time, the evaporation of fuel is an endothermic process, while heat exchange also occurs between the surrounding environment and fire flame kernel. Under this counteraction, the size of the initial flame kernel gradually decreases, and its brightness also gradually decreases. This process is the key to determine whether the ignition is successful. If the heat absorption rate of ambient circumstance is higher than the heat liberation rate of flame kernel, the flame kernel is about to extinguish. After the heat liberation

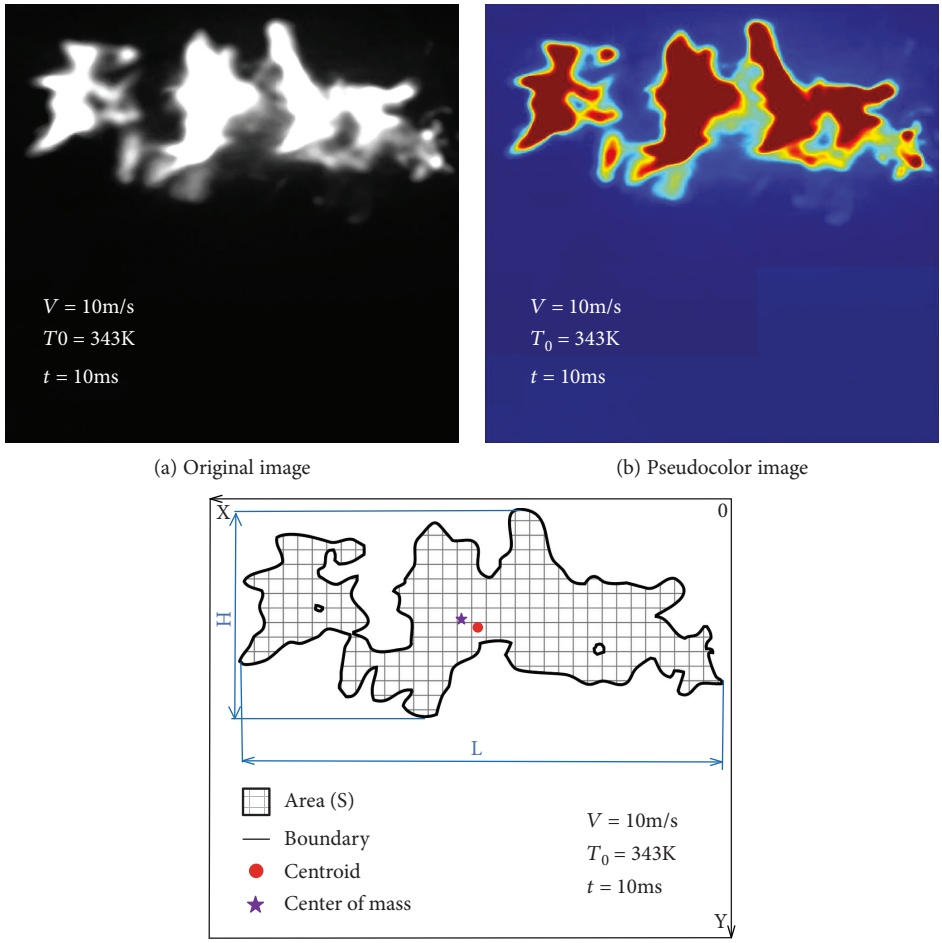

(a) Original image

(b) Pseudocolor image

(c) Image boundary

Figure 4: Image processing method.

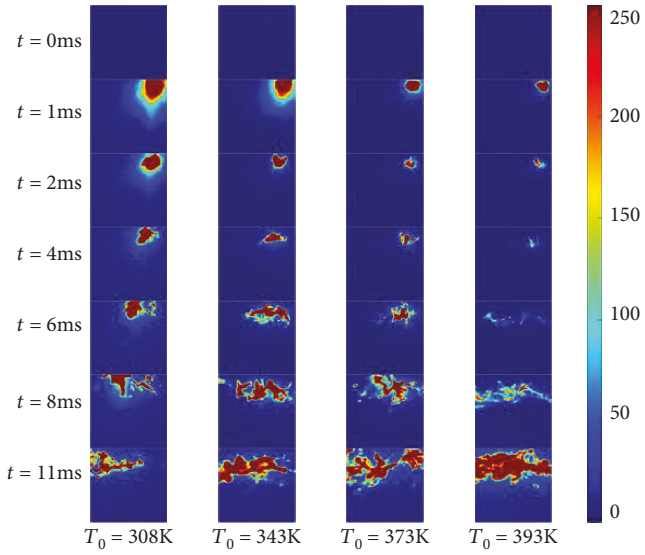

Figure 5: Initial flame kernel formation and flame propagation.

rate increased, the size of flame kernel gradually increases, and the brightness is enhanced, forming the flame and indicating the success of combustor ignition. With the increasing airflow temperature, the decrease in size and brightness becomes clearer during the development of initial flame kernel. However, the brightness of the region where the flame is eventually formed gradually increased. This is because the airflow density gradually decreased as the airflow temperature increased. Meanwhile, the gradually increased evaporation rate of fuel creates a higher fuel/air ratio near the spark plug. At the same time, both the combustion and the heat liberation rates of flame increase with the higher evaporation rate of fuel.

The flame profile at 11 ms under different airflow temperatures is shown in Figure 6. The flame length and height increases with the increase of airflow temperature, which shows that the increase of airflow temperature accelerates the propagation velocity. This is because the evaporation rate of fuel and chemical reaction rate increase with the increase of airflow temperature, which promotes the accelerated propagation of flame.

For the flame development under normal circumstances, the flame area gradually increased, exhibiting a constant increase in the bright regions of image. The digital image is composed of countless pixels, and the area of each pixel is equal. Therefore, in image processing, the area can be calculated by binarizing the image, segmenting the target object,

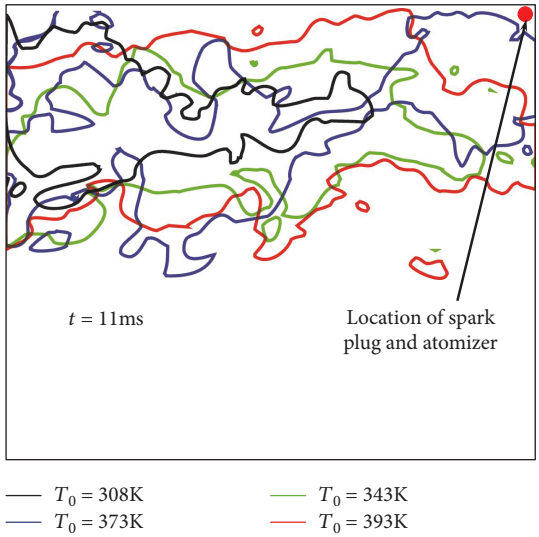

Figure 6: Influence of airflow temperature on flame structure.

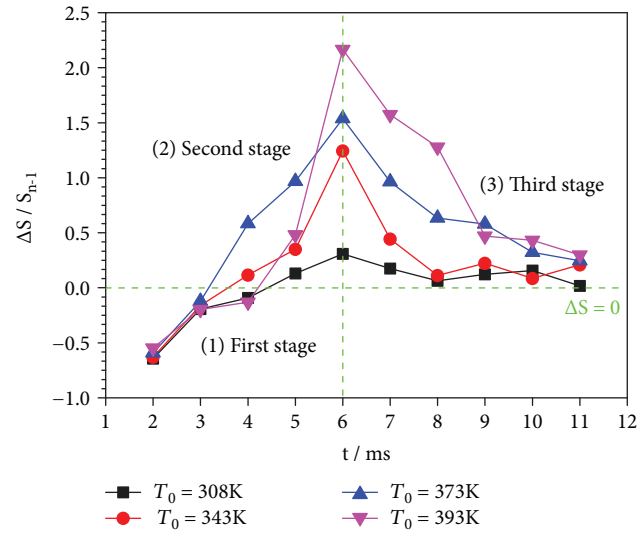

Figure 7: Effect of air temperature on the growth rate of flame area.

and then counting the total number of pixels. The formula can be expressed as follows:

$$S = S_i \times \sum I_i, \tag{1}$$

where S is the total area of target object; S_i is the area of a single pixel point; I_i is the pixel in the target object region (the point has a value of 1 in the binary image). In addition, during the combustion, the variation rate of flame area directly reflects the variation trend of heat liberation rate of flame. In this study, the growth rate of flame area was used to indicate the magnitude of combustion rate of flame. The variation rate of flame area of 11 consecutive frames was calculated, as shown in Figure 7. In the calculation, the target area of the first frame image ($t = 1$ ms) was used as the starting reference object. The calculation formula can be expressed as follows:

$$\frac{\Delta S}{S_{n-1}} = \frac{S_n - S_{n-1}}{S_{n-1}}, \tag{2}$$

where $\Delta S/S_{n-1}$ is the growth rate of flame area; S_n is the flame area in the n^{th} frame image; S_{n-1} is the flame area in the $(n-1)^{\text{th}}$ frame image.

The variation rate of flame area has the same development process during the ignition, as shown in Figure 7. When the initial flame kernel forms, the flame kernel first undergoes area reduction, but its negative growth rate gradually decreases. Subsequently, the area exhibits a rapid increase, exhibiting a rapid increase in the growth rate of area and soon reaching the maximum growth rate. Finally, the area continues to increase, but the growth rate gradually decreases. Therefore, the growth rate of area gradually decreases even though it is positive. Therefore, the ignition process can be divided into three stages according to the growth rate of flame area. (1) Formation stage of initial flame kernel: this refers to the stage before the growth rate of area has a negative increase. During this stage, the heat released by initial flame kernel is mainly used to evaporate the fuel for accelerating the combustion reactions. (2) Rapid development stage of flame: this refers to the period from the moment of achieving a positive growth to the moment of reaching the maximum growth rate. After the formation of initial flame kernel, the higher heat liberation intensity accelerates the fuel's evaporation, further increasing the heat liberation intensity of flame. Under the action of such a positive feedback, the chemical reaction rate of flame increases rapidly, exhibiting a rapid increase in the area of flame. (3) Steady development of the flame: this refers to the declining stage of growth rate of flame area. In this stage, both the rapid evaporation of small droplets and the constant evaporation of large droplets participate in combustion, exhibiting a gradually expanded flame area but decreased area growth rate. Although the variation in airflow temperature affects the entire ignition, the effects are clearer for the first and second stages. During the first stage, with the increase in airflow temperature ($T_0 = 308$–373 K), the formation time of initial flame kernel gradually decreases. However, as the airflow temperature further increases ($T_0 = 393$ K), the formation time of initial flame kernel increases. In the second stage, with the increase in airflow temperature, the slope of growth curve of area rapidly increases and the growth rate of flame area also rapidly increases.

The flame has a 3D structure and continually stretched and deformed during its development. The ratio of surface area and volume can be used to evaluate the heat liberation intensity of flame. The image shows the flame's structural characteristics in a 2D format, namely, the projection of a 3D flame on a 2D plane. Therefore, the ratio of perimeter of flame boundary contour and flame area can be used to evaluate the heat liberation intensity of flame, as shown in Figure 8.

Through a binary processing of image, extraction of target boundary, and counting the total number of pixels at the boundary line, the contour perimeter of flame boundary

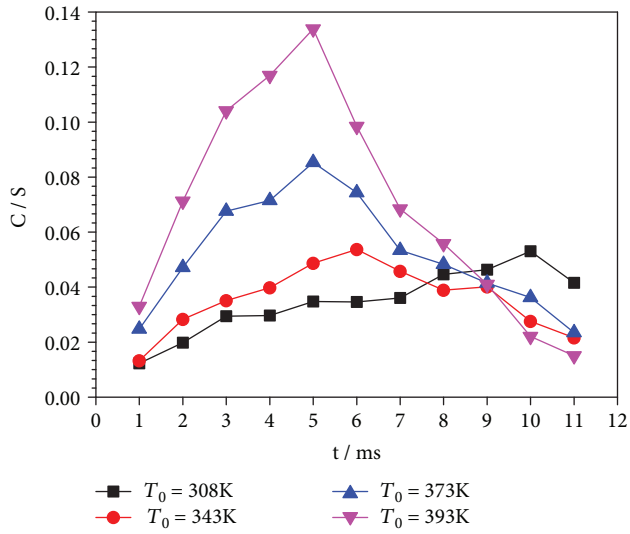

FIGURE 8: Perimeter-to-area ratio at flame development process.

can be obtained. The calculation formula can be expressed as follows:

$$C = L_i \times \sum I_i, \tag{3}$$

where C is the perimeter of target boundary, L_i is the length of a single pixel, and I_i is the number of pixels at the boundary of target.

The change in airflow temperature significantly affects the heat liberation intensity during the flame development, as shown in Figure 8. Although the heat liberation intensity first increases and then decreases after the initial flame kernel is formed, the increase in heat liberation intensity and peak value are both lower when the airflow temperatures were $T_0 = 308$ K and $T_0 = 343$ K. When the airflow temperatures were $T_0 = 373$ K and $T_0 = 393$ K, the heat liberation intensity of flame rapidly increases and has a higher peak value, with a concrete representation of the steeper slope of perimeter-to-area ratio curve. As the inlet temperature increases, the slope increases, and the peak value also increases. A comparison between the initial heat liberation intensity of initial flame kernel ($t = 1$ ms) under four inlet airflow temperatures indicates that the heat liberation intensity of initial flame kernel gradually increases with the increase in inlet temperature.

During the combustion, the flame is continuously stretched along the axial direction under the action of airflow. In addition, a concentration gradient of fuel exists in the circumferential direction of combustor; therefore, the flame expands in the circumferential direction at the same time. The flame image shows the projection of a 3D flame on the 2D plane. Therefore, the length-to-height ratio not only characterizes the axial and radial expansion extents of flame at each moment but also reflects the main factors influencing the deformation of flame. Owing to the irregular shape of flame, the local deformation characteristics of flame can be represented by the maximum length-to-height ratio on the contour line of flame, as shown in Figure 9(a). However, the local maximum characteristics cannot satisfactorily reflect the overall deformation of flame. Therefore, the equivalent mean length-to-height ratio of flame was used, as shown in Figure 9(b). The equivalent mean approach considered the irregular figure as a regular ellipse. The major and minor axes of the ellipse were used to represent the mean length and height of the original image, respectively. The selection of ellipse is based on the principle that the selected ellipse has an equal second-order central momentum with the original figure, i.e.,

$$\mathrm{Var}(x) = \int_{-\infty}^{\infty} \left[x - E(x)^2\right] f(x)\,dx. \tag{4}$$

Figure 9 shows that the development trends of maximum and mean length-to-height ratio curves are exactly the same. Both the curves first increased and then decreased, and their values are both more than 1. The results show that the force of airflow on the flame is the main factor that increases the flame area and heat liberation. With the passing of time, the evaporation rate of fuel gradually increases, and the fuel concentration gradient in the combustor increases. Therefore, the radial diffusion extent of flame is gradually intensified. Furthermore, the peak points shown in the two figures are the same, i.e., the moment of peak point is shortened with the increase in inlet temperature, and the peak value clearly increases when the inlet temperature is higher than 343 K. The results show that an increase in the airflow temperature increases the circumferential concentration gradient within the combustor, thus increasing the stretching rate of flame and inducing the radial expansion of flame in advance. Although the curves in the two figures show the same characteristics, some differences were also observed. This clearly indicates that the mean length-to-height ratio is higher than the maximum length-to-height ratio at each moment, indicating that the boundary wrinkles of flame can be mainly attributed to the stretching of the entire flame under the action of airflow.

Centroid refers to the geometric center of an object. The centroid concept was applied in the processing of flame image, where the moving trajectory of flame centroid in an image was used to identify the developing direction, as shown in Figure 10(a). The centroid of binary image can be calculated as follows:

$$\begin{aligned} x &= \frac{1}{n}\sum x_i, \\ y &= \frac{1}{n}\sum y_i, \end{aligned} \tag{5}$$

where x and y are the horizontal and vertical coordinates of centroid; x_i and y_i are the horizontal and vertical conditions of each pixel within the flame region; n is the number of pixels within the flame region.

In turbulent nonpremixed combustion, the evaporation and blending processes of fuel result in the uneven concentration distribution of fuel in the combustor, i.e., the uneven distribution of fuel/air ratio. In the image of flame, the uneven distribution is presented as the uneven distribution

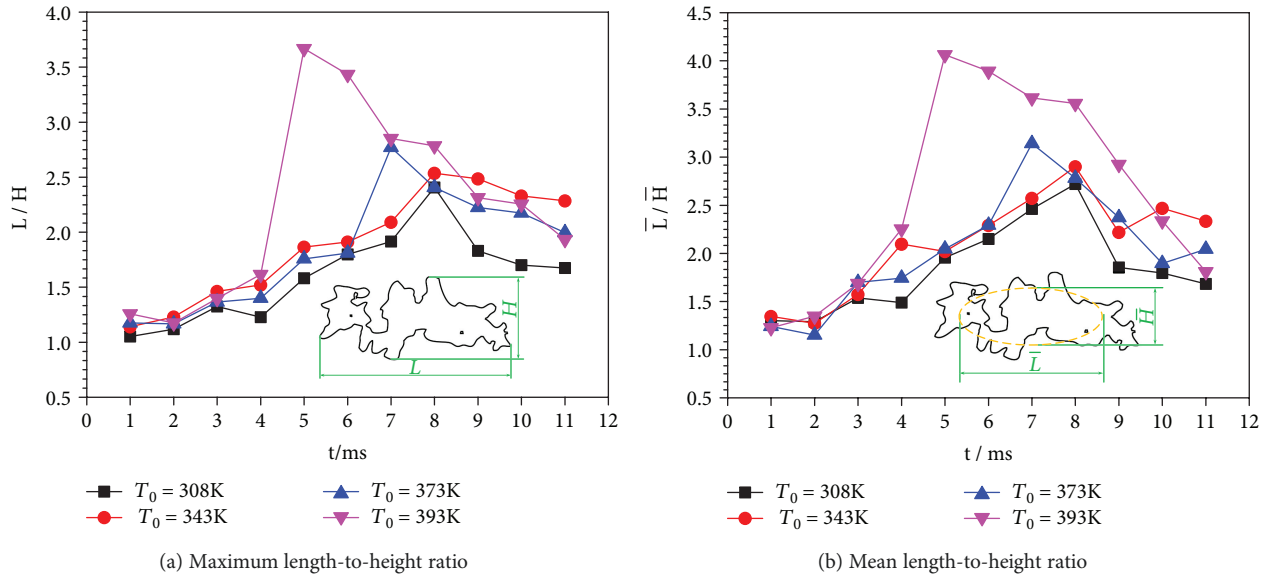

(a) Maximum length-to-height ratio (b) Mean length-to-height ratio

Figure 9: Length-to-height ratio at flame development process.

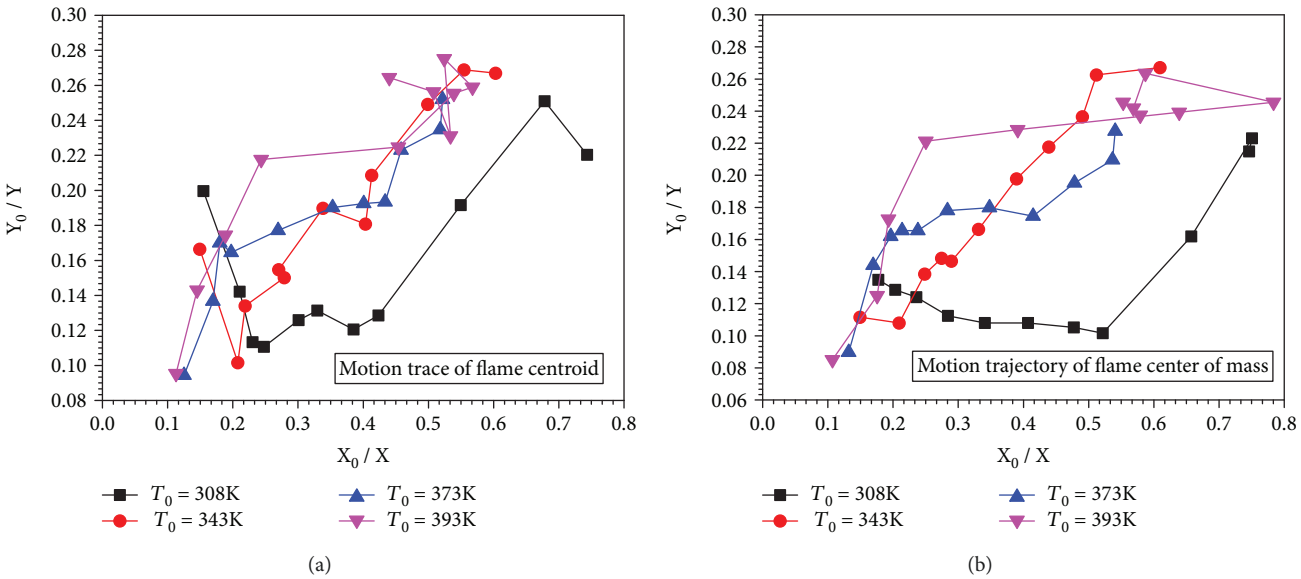

(a) (b)

Figure 10: Motion trajectory of flame center.

in brightness. If the bright distribution in image is assumed to be the mass distribution, the position of mass center of flame, namely, the center of brightness distribution at different moments can be calculated using the weighting method on brightness, as shown in Figure 10(b). The mass center of gray image can be calculated as follows:

$$x = \frac{1}{N}\sum x_i \cdot I_{xi},$$
$$y = \frac{1}{N}\sum y_i \cdot I_{yi}, \quad (6)$$

where x and y are the horizontal and vertical coordinates of mass center; x_i and y_i are the horizontal and vertical coordinates of each pixel within the flame region; I_{xi} and I_{yi} are the brightness corresponding to the coordinates of x_i *and* y_i, respectively. N is the number of pixels within the flame region.

As shown in Figure 10, the fuel concentration distribution and gradient are not uniform under the action of airflow, indicating that the flame has a simultaneous and irregular development along the axial and radial directions of combustor at different moments. This clearly shows that the positions of mass center and centroid of flame are irregular at each moment, indicating the characteristics of turbulent nonpremixed combustion. However, in general, the axial moving distances of centroid and mass center of the flame are much longer than those along the radial direction, but their positions at each moment are not the same. With a

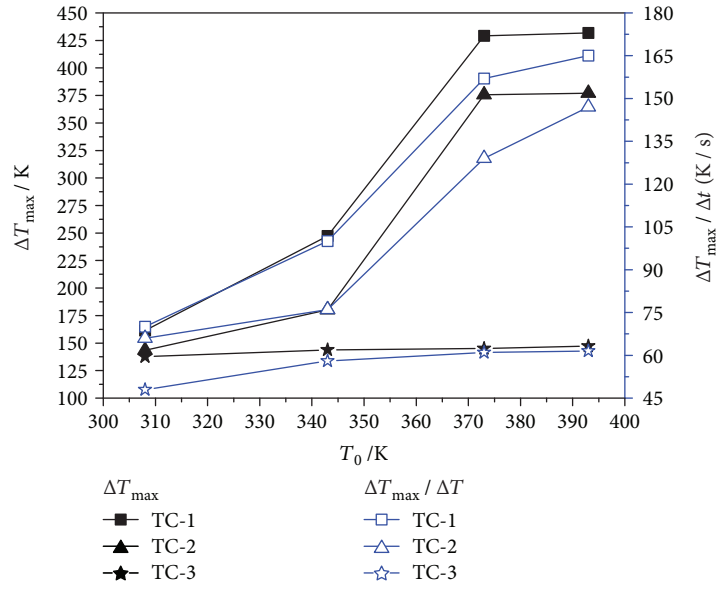

Figure 11: Effect of airflow temperature on the maximum temperature increase and maximum rate of temperature increase at combustor exit.

higher airflow temperature, the radial moving distance has an increasing trend, while the axial distance of the final flame ($t = 11$ ms) has a decreasing trend. In addition, as the temperature of airflow increases, the centroid and mass center of initial flame kernel gradually move closer to the center of the end face of nozzle (coordinates: $X_0/X = 0.09$, $Y_0/Y = 0.03$). The results show that as the temperature of airflow increases, the reaction zone of initial flame kernel advances. When the air temperatures were $T_0 = 308$ K and $T_0 = 343$ K, the centroid and mass center of initial flame kernel first showed a clear upward movement to the upper side of combustor. When the air temperatures were $T_0 = 373$ K and $T_0 = 393$ K, the centroid and mass center of initial flame kernel clearly moved to the bottom of the combustor. When the air temperature was $T_0 = 393$ K, the centroid and mass center of flame showed the "back-return" characteristic after $t = 8$ ms, indicating that although the positions of mass center and centroid are not the same, their macroscopic moving trends are almost the same.

The values of temperature increase and increase rate reflect the increase level of combustion temperature and magnitude of heat liberation rate of combustion, respectively. Therefore, they are the critical factors that determine whether the ignition in a combustor is successful, as shown in Figure 11. The variation trends of maximum temperature increase (ΔT_{max}) measured using the thermocouples at 1/4H and 1/2H (TC-1 and TC-2) are almost consistent, both exhibiting a rapid increase with the increase in inlet air temperature and then remaining constant. However, the curve of maximum temperature increase rate ($\Delta T_{max}/\Delta t$) exhibits a constant increase. As the inlet temperature of combustor increased from 308 K to 373 K, the maximum temperature increase of TC-1 increased from 161.4 K to 429.1 K, and the maximum rate of temperature increase increased from 70 K/s to 157 K/s. As the inlet temperature increased from 373 K to 393 K, the variations in maximum temperature increase of TC-1 and TC-2 were not clear. For instance, the ΔT_{max} of TC-1 slightly increased from 429.1 K to 431.9 K, while that of TC-2 slightly increased from 375.7 K to 377 K. The $\Delta T_{max}/\Delta t$ increased constantly, where TC-1 increased from 157 K/s to 165 K/s, while TC-2 increased from 129 K/s to 147 K/s, but with a lower increasing rate. For the thermocouple (TC-3) at a radial distance of 3/4H, the ΔT_{max} and $\Delta T_{max}/\Delta t$ are both stable, only increasing from 137.6 K and 48 K/s to 147.2 K and 61.5 K/s, respectively. This indicates that with the increase in airflow temperature, the evaporation rate of fuel increases; the combustion temperature and heat liberation rate increase accordingly. However, a gradual increase in the fuel/air ratio leads to a lower maximum temperature increase and a slower increase in temperature increase rate. In addition, the ΔT_{max} and $\Delta T_{max}/\Delta t$ of TC-3 are relatively low, indicating that the radial development of flame does not reach half of the height of combustor, where the temperature change is affected by heat radiation. According to the flow characteristics of combustor, the positions of combustion regions are mainly determined by the fuel/air distribution caused by the airflow.

The Δt_{start} of thermocouple at the outlet of combustor is defined as the time difference between the discharge moment of spark plug and starting moment of temperature increase; the Δt_{max} of thermocouple is defined as the time difference between the discharge moment of spark plug and the moment when the temperature of thermocouple reaches the maximum value, as shown in Figure 12. As the airflow temperature increases, the Δt_{start} starts to increase rapidly within $T_0 = 308$–343 K, and Δt_{max} slightly increases. For the temperature range of $T_0 = 343$–373 K, the Δt_{start} slightly increases, while the Δt_{max} increases rapidly. When the temperature range was $T_0 = 373$–393 K, the Δt_{start} started to decrease rapidly, but the Δt_{max} slightly increased. In particular, TC-3 has

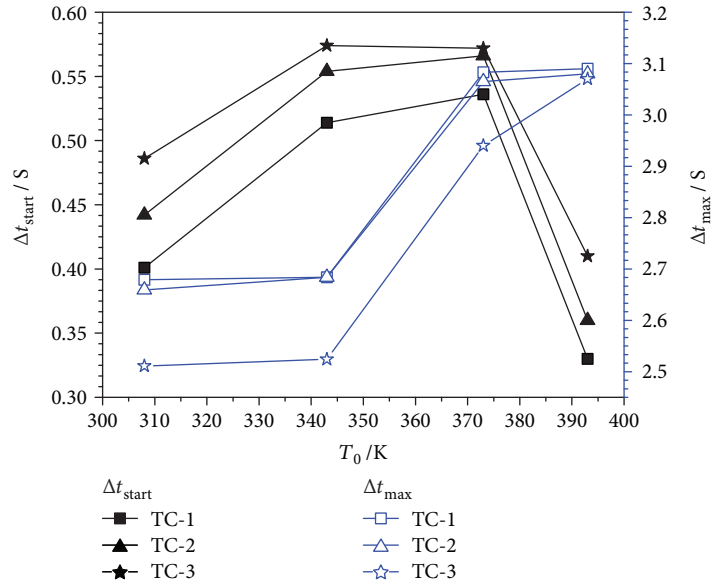

Figure 12: Effect of airflow temperature on the temperature response time at combustor exit.

a more clear variation trend. In addition, with the increase in radial distance from the outlet thermocouple, Δt_{start} increases, while Δt_{max} decreases. The thermal response time of thermocouple is mainly affected by the heat transfer rate of the surrounding medium. The higher the heat transfer rate, the shorter the thermal response time. Therefore, the starting moment of temperature increase reflects the heat liberation intensity of nucleus in the first stage during the ignition, whereas the maximum temperature increase time reflects the continuous heat liberation intensity of the flame after the fuel supply is stopped. During the first stage of ignition, the heat liberation intensity of initial flame kernel increases constantly after the initial flame kernel is formed, and the intensity significantly increases with the increase in airflow temperature, as shown in Figure 8. However, the increase in ambient temperature leads to the decrease in heat transfer rate. Therefore, it can be concluded from the Δt_{start} curve that, when $T_0 = 308$–373 K, the heat liberation intensity of flame kernel increases with the increase in airflow temperature, but the heat exchange rate with the environment tends to decrease with a decreasing trend. When T_0 was 393 K, the heat liberation intensity of flame kernel significantly increased, and the heat exchange rate with the environment rapidly increased, indicating the rapid decline of Δt_{start}. It can also be concluded that an airflow temperature more than 373 K has a qualitative improvement on the success rate of ignition. When the fuel supply is stopped, on the one hand, there is still incompletely consumed fuel in the combustor; therefore, a concentration gradient exits. On the other hand, the high-temperature flame has a thermal inertia; therefore, the outlet temperature will continue to increase. When the airflow temperature increases, the evaporation rate of fuel increases, and subsequently the ignition fuel/air ratio also increases. The amount of incompletely burned fuel increases when the fuel supply is stopped. Therefore, Δt_{max} gradually increases with the increase in airflow temperature.

4. Conclusions

Under atmospheric pressure conditions with an airflow rate of 10 m/s and fuel flow rate of 1.24 g/s, the effect of different airflow temperatures ($T_0 = 308$ K, 343 K, 373 K, and 393 K) on the morphology of flame in spray ignition was evaluated. In the experiments, the ignition and fuel supply systems were synchronously controlled using a PLC. The internal triggering method was used to couple the high-speed camera and thermocouple at the outlet, and the development of flame and temperature variation at the outlet of combustor was simultaneously recorded. MATLAB software was used to process the images of flame and to evaluate the effect of airflow temperature on the flame morphology during its development. The main results of investigation are as follows:

(1) According to the variation of growth rate of flame area during the development, the ignition process can be divided into three stages: (i) formation of initial flame kernel, (ii) rapid development of flame, and (iii) stable development of flame

(2) With the increase in airflow temperature, the heat release intensity of initial flame kernel increases, and the ratio of perimeter to area as a characterization parameter increased by 8%, 86%, and 33%, respectively. During the development, the heat release intensity showed a rapid upward trend and rapidly reached the maximum

(3) With the increase in heat release intensity, the flame exhibited an intense deformation, including axial stretching under the action of airflow and radial diffusion due to the concentration gradient of fuel. The values of maximum length-to-height ratio and equivalent mean length-to-height ratio were more than 1 at each moment, but the equivalent mean

length-to-height ratio was greater than the maximum length-to-height ratio

(4) The movements of centroid and mass center of flame are irregular, and their positions are not the same at any moment. However, their macroscopic moving trends are consistent. With the increase in airflow temperature, the centroid and mass center of initial flame kernel are both closer to the center of end-face of spark plug

(5) With the increase in airflow temperature, the time difference corresponding to the maximum temperature increase of the outlet thermocouple all increased, but the time difference for the starting moment of temperature increase first increased and then decreased

(6) With the increase in airflow temperature, the maximum temperature rise of outlet increased by about 53%, 73.5%, and 0.65%, respectively. Meanwhile, the maximum rate of temperature rise increased by about 42.8%, 57%, and 5.1%, respectively

Data Availability

The data used to support the findings of this study are available from the corresponding author upon request.

Conflicts of Interest

The authors declare that they have no conflicts of interest.

Acknowledgments

This work was supported by "the National Natural Science Foundation of China", No. 51476077.

References

[1] E. Mastorakos, "Forced ignition of turbulent spray flames," *Proceedings of the Combustion Institute*, vol. 36, no. 2, pp. 2367–2383, 2017.

[2] S. K. Aggarwal, "Single droplet ignition: theoretical analyses and experimental findings," *Progress in Energy and Combustion Science*, vol. 45, pp. 79–107, 2014.

[3] B. Sforzo, H. Dao, S. Wei, and J. Seitzman, "Liquid fuel composition effects on forced, non-premixed ignition," in *Proceedings of the ASME Turbo Expo: Turbine Technical Conference and Exposition*, vol. 4A, Seoul, South Korea, June 2016.

[4] S. F. Ahmed, R. Balachandran, T. Marchione, and E. Mastorakos, "Spark ignition of turbulent non-premixed bluff-body flames," *Combustion and Flame*, vol. 151, no. 1-2, pp. 366–385, 2007.

[5] M. Epaminondas, "Ignition of turbulent non-premixed flames," *Progress in Energy and Combustion Science*, vol. 35, no. 1, pp. 57–97, 2009.

[6] S. Choi, D. Lee, and J. Park, "Ignition and combustion characteristics of the gas turbine slinger combustor," *Journal of Mechanical Science and Technology*, vol. 22, no. 3, pp. 538–544, 2008.

[7] H. Bao, J. Zhou, and Y. Pan, "The effect of kerosene injection on ignition probability of local ignition in a scramjet combustor," *Acta Astronautica*, vol. 132, pp. 54–58, 2017.

[8] A. Larsson, A. Berg, and A. Bonaldo, "Fuel flexibility at ignition conditions for industrial gas turbines," in *ASME Turbo Expo 2013: Turbine Technical Conference and Exposition*, p. 6, San Antonio, Texas, USA, 2013.

[9] B. Peterson, D. L. Reuss, and V. Sick, "On the ignition and flame development in a spray-guided direct-injection spark-ignition engine," *Combustion and Flame*, vol. 161, no. 1, pp. 240–255, 2014.

[10] S. Brieschenk, Q. Pontalier, A. Duffaut et al., "Characterization of a spark ignition system for flameholding cavities," in *45th AIAA Plasmadynamics and Lasers Conference*, pp. 1–18, Atlanta, GA, Georgia, 2014.

[11] A. L. H. Duque and W. L. Perry, "Electromagnetic enhanced ignition," *Combustion and Flame*, vol. 181, pp. 16–21, 2017.

[12] W. P. Jones and A. Tyliszczak, "Large eddy simulation of spark ignition in a gas turbine combustor," *Flow Turbulence Combust*, vol. 85, no. 3-4, pp. 711–734, 2010.

[13] K. Truffin, C. Angelberger, S. Richard, and C. Pera, "Using large-eddy simulation and multivariate analysis to understand the sources of combustion cyclic variability in a spark-ignition engine," *Combustion and Flame*, vol. 162, no. 12, pp. 4371–4390, 2015.

[14] V. Subramanian, P. Domingo, and L. Vervisch, "Turbulent flame spreading mechanisms after sparking ignition," *AIP Conference Proceedings*, vol. 1190, pp. 68–89, 2009.

[15] S. Fontanesi, A. d'Adamo, and C. J. Rutland, "Large-eddy simulation analysis of spark configuration effect on cycle-to-cycle variability of combustion and knock," *International Journal of Engine Research*, vol. 16, no. 3, pp. 403–418, 2015.

[16] M. A. Soroudi, E. Mollahasanzadeh, and N. Rasooli, "Prediction of spark ignition performance in an industial gas turbine combustor," in *Proceedings of the European Combustion Meeting*, pp. 1–20, Budapest, Hungary, 2015.

[17] D. W. Naegeli and L. G. Dodge, "Ignition study in a gas turbine combustor," *Combustion Science and Technology*, vol. 80, no. 4–6, pp. 165–184, 1991.

[18] S. F. Ahmed and E. Mastorakos, "Spark ignition of lifted turbulent jet flames," *Combustion and Flame*, vol. 146, no. 1-2, pp. 215–231, 2006.

[19] T. Marchione, S. F. Ahmed, and E. Mastorakos, "Ignition of turbulent swirling n-heptane spray flames using single and multiple sparks," *Combustion and Flame*, vol. 156, no. 1, pp. 166–180, 2009.

[20] E. Mastorakos, "Spark ignition of turbulent non-premixed flames: experiments and simulations," *American Institute of Physics Conference Series*, vol. 199, no. 1, pp. 63–67, 2009.

[21] E. Oldenhof, M. J. Tummers, E. H. van Veen, and D. J. E. M. Roekaerts, "Ignition kernel formation and lift-off behaviour of jet-in-hot-coflow flames," *Combustion and Flame*, vol. 157, no. 6, pp. 1167–1178, 2010.

[22] J. Chen, J. Li, and L. Yuan, "Effects of inlet pressure on ignition of spray combustion," *International Journal of Aerospace Engineering*, vol. 2018, Article ID 3847264, 13 pages, 2018.

[23] S. K. Aggarwal, "A review of spray ignition phenomena: present status and future research," *Progress in Energy and Combustion Science*, vol. 24, no. 6, pp. 565–600, 1998.

[24] D. J. Valco, M. J. Tess, J. E. Temme et al., "Ignition characterization of F-76 and algae-derived HRD-76 at elevated temperatures and pressures," *Combustion and Flame*, vol. 181, pp. 157–163, 2017.

[25] V. Vukadinovic, P. Habisreuther, and N. Zarzalis, "Influence of pressure and temperature on laminar burning velocity and Markstein number of kerosene Jet A-1. Experimental and numerical study," *Fuel*, vol. 111, pp. 401–410, 2013.

[26] M. Li, C. Wang, H. Sun, H. Liu, S. Yang, and A. Zhang, "Heat and mass transfer of flame spread over jet fuel at sub-flash temperature," *Experimental Thermal and Fluid Science*, vol. 89, pp. 276–283, 2017.

[27] A. H. Lefebvre, *Gas Turbine Combustion*, CRC Press, New York, NY, USA, 1998.

[28] X. Wang, C. Wang, K. Zhou et al., "Experimental study on combustion behaviors and carbon monoxide emission characteristics of single coal pellets," *Journal of Energy Engineering*, vol. 144, no. 5, 2018.

[29] B. Chehroudi, "Recent experimental efforts on high-pressure supercritical injection for liquid rockets and their implications," *International Journal of Aerospace Engineering*, vol. 2012, Article ID 121802, 31 pages, 2012.

[30] R. Hernandez and J. Ballester, "Flame imaging as a diagnostic tool for industrial combustion," *Combustion and Flame*, vol. 155, no. 3, pp. 509–528, 2008.